JPn Neuroscience

The Journal of Physiology

J Physiol 590.22 (2012) pp 5895–5905

Zinc induces long-term upregulation of T-type calcium current in hippocampal neurons *in vivo*

Dana Ekstein[1,2], Felix Benninger[1], Moshe Daninos[1], Julika Pitsch[3], Karen M. J. van Loo[3], Albert J. Becker[3] and Yoel Yaari[1,4]

[1]*Department of Medical Neurobiology, IMRIC, Hebrew University-Hadassah School of Medicine, Jerusalem 91120, Israel*
[2]*Department of Neurology, Hadassah Hebrew University Medical Center, Jerusalem 91120, Israel*
[3]*Department of Neuropathology, University of Bonn Medical Center, Bonn, Germany D-53127*
[4]*The Interdisciplinary Center for Neuronal Computation, Hebrew University, Jerusalem 91904, Israel*

Key points

- Zinc induces various acute and persistent effects in neurons and it acutely blocks T-type voltage-gated calcium current (I_{CaT}).
- I_{CaT} contributes to pilocarpine status epilepticus (SE)-induced epileptogenesis (transformation of normal brain into epileptic) by mediating the increase in intrinsic excitability of CA1 hippocampal neurons. Therefore, since SE causes both zinc release into the extracellular space and long-lasting increase in I_{CaT}, zinc may actually upregulate I_{CaT} on the long-term.
- We demonstrated that when injected into the lateral ventricles of rats zinc upregulated I_{CaT} in a subset of CA1 hippocampal neurons for about 2 weeks.
- This shows that zinc has a dual effect on I_{CaT}, blocking it acutely while causing its long-term upregulation.
- This finding provides a possible explanation to the mechanism of epileptogenesis induced by pathological conditions associated with enhanced release of zinc, such as SE.

Abstract Extracellular zinc can induce numerous acute and persistent physiological and toxic effects in neurons by acting at their plasma membrane or intracellularly following permeation or uptake into them. Zinc acutely and reversibly blocks T-type voltage-gated calcium current (I_{CaT}), but the long-term effect of zinc on this current has not been studied. Because chemically induced status epilepticus (SE) results in the release of zinc into the extracellular space, as well as in a long-lasting increase in I_{CaT} in CA1 pyramidal cells, we hypothesized that zinc may play a causative role in I_{CaT} upregulation. We tested this hypothesis by monitoring for 18 days the effects of zinc and ibotenic acid (a neurotoxic agent serving as control for zinc), injected into the right lateral ventricle, on I_{CaT} in rat CA1 pyramidal cells. Both zinc and ibotenic acid caused marked hippocampal lesions on the side of injection, but only minor damage to contralateral hippocampi. Zinc, but not ibotenic acid, caused upregulation of a nickel-sensitive I_{CaT} in a subset of contralateral CA1 pyramidal cells, appearing 2 days after injection and lasting for about 2 weeks thereafter. In contrast, acute application of zinc to CA1 pyramidal cells promptly blocked I_{CaT}. These data indicate that extracellular zinc has a dual effect on I_{CaT}, blocking it acutely while causing its long-term upregulation. Through the latter effect, zinc may regulate the intrinsic excitability

D. Ekstein and F. Benninger contributed equally to this work.

DOI: 10.1113/jphysiol.2012.242537

of principal neurons, particularly in pathological conditions associated with enhanced release of zinc, such as SE.

(Resubmitted 6 August 2012; accepted 22 August 2012; first published online 28 August 2012)

Corresponding author D. Ekstein: Department of Neurology, P.O.B. 12000, Hadassah-Hebrew University Medical Center, Jerusalem, Israel 91120. Email: dekstein@hadassah.org.il

Abbreviations aCSF, artificial cerebrospinal fluid; I_{CaT}, T-type calcium current; I.C.V., intracerebroventricular; MTF-1, metal transcription factor 1; NeuN, neuronal nuclei; PBS, phosphate-buffered saline; SE, status epilepticus.

Introduction

Brain neurons contain large amounts of loosely and tightly bound zinc contributing to their normal function (Frederickson *et al.* 2005; Sensi *et al.* 2009). Several studies have suggested that loosely bound zinc present in a subset of glutamatergic nerve terminals is co-released with glutamate into the synaptic cleft. Although the amount of released zinc that actually reaches postsynaptic membranes is not known, its binding to neuronal plasma membrane receptors and ion channels may modulate numerous neuronal and synaptic functions (Vogt *et al.* 2000; Molnar & Nadler, 2001; Besser *et al.* 2009; Sensi *et al.* 2009; but see Kay & Toth, 2006; Evstratova & Toth, 2011). Furthermore, increase in the concentration of intracellular zinc by either penetration of extracellular zinc or release from internal binding sites (Cuajungco & Lees, 1998) can modify cellular metabolism, inducing neuronal cell death at toxic levels (Choi & Koh, 1998; Park *et al.* 2000), but also mediating neuroprotection in other cases (Lee *et al.* 2008). Additionally, it can affect transcription of many cellular proteins, mainly through its binding to metal transcription factor 1 (MTF-1; Cousins *et al.* 2006). Through these multiple acute and persistent effects, zinc likely plays a role in normal and pathological brain plasticity (Nakashima & Dyck, 2009; Sensi *et al.* 2009).

Zinc has also been shown to regulate conductivity through both native (Nelson *et al.* 2007) and recombinant T-type voltage-gated calcium channels (Traboulsie *et al.* 2007). The native T-type calcium channels ubiquitously expressed in brain neurons, as well as in many peripheral tissues, comprise three isoforms, namely, $Ca_V3.1$, $Ca_V3.2$ and $Ca_V3.3$, which generate low threshold-activated, inactivating calcium currents (I_{CaT}; Perez-Reyes, 2003). In particular, zinc potently blocks $Ca_V3.2$ channels (IC_{50} 0.8 μM; Traboulsie *et al.* 2007) by binding to the same site that is responsible for their potent inhibition by low concentrations of nickel (Kang *et al.* 2010). Zinc also has a blocking effect on $Ca_V3.1$ and $Ca_V3.3$ channels, albeit less potent than on $Ca_V3.2$ (IC_{50} 100- and 200-fold higher, respectively). In addition, it slows the deactivation of $Ca_V3.3$ channels. These effects of zinc are acute and reversible upon wash (Traboulsie *et al.* 2007). Whether zinc also exerts long-term effects on neuronal T-type calcium channels has not been investigated to date. It is interesting to note, however, that chemically induced status epilepticus (SE) causes accumulation of free zinc in somata of CA1 pyramidal cells (Suh *et al.* 2001) and induces neurodegeneration (Qian *et al.* 2011). Shortly thereafter, $Ca_V3.2$ expression and I_{CaT} amplitude in these neurons are strongly upregulated for several weeks (Su *et al.* 2002; Becker *et al.* 2008). These observations prompted us to test whether the increase in I_{CaT} is causally related to exposure of these neurons to zinc. Here we have tested this hypothesis by monitoring the properties of I_{CaT} in CA1 pyramidal cells during 18 days that follow intracerebroventricular (I.C.V.) zinc administration. Our data suggest that exposing neurons to zinc can induce a long-term increase in I_{CaT}.

Methods

I.C.V. injections

All animal experiments were conducted in accordance with the guidelines of the Animal Care Committee of the Hebrew University. Adult male Sabra rats (Lutsky *et al.* 1984; 150–250 g), under intraperitoneally administered pentobarbital anaesthesia (40 mg kg^{-1}), were positioned in a stereotactic frame (TSE Systems, Bad Homburg, Germany). Injections into the right ventricles were made at the following coordinates in relation to Bregma: 0.8 mm posterior; 1.4 mm to the right; and 5 mm beneath the calvarium using a continuous cycle syringe pump (TSE Systems). We used three injection protocols modified to obtain comparable hippocampal damage with zinc and ibotenic acid (see Results): 15 μl of normal saline over 90 min (*saline-injected* animals); 15 μl of normal saline containing 45 μg $ZnCl_2$ (22 mM) over 90 min (*zinc-injected* animals); and 10 μl of normal saline containing 2 μg ibotenic acid (1.3 mM) over 30 min (*ibotenic acid (ibotenate)-injected* animals).

Histological analyses

Rats were decapitated under deep isofluorane anaesthesia, and their brains were quickly removed and stored in 4% paraformaldehyde. Coronal paraffin sections, 4 μm, were deparaffinized in xylene, rehydrated in graded alcohols, and washed in Tris-buffer. The extent of hippocampal neuronal cell loss was assessed in slices

immunolabeled with antibodies against neuronal nuclei (NeuN), as previously described (Becker *et al.* 2008). For immunolabeling, endogenous peroxidase activity was quenched by incubation in phosphate-buffered saline (PBS) containing 1% hydrogen peroxide. Heat treatment resulted in antigen unmasking, followed by blocking of non-specific binding performed with 0.5% normal goat serum for 2 h at 37°C. Primary antibodies were added before incubation of slides overnight at room temperature. Sections were washed in PBS, covered with diluted biotinylated secondary antibody, and incubated for 2 h at 37°C. An avidin–biotin complex was applied (Vector Laboratories, Burlingame, CA, USA) and visualized using a diaminobenzidine solution (1 : 50 DAB, containing 0.05% H_2O_2). Haematoxylin-counterstained sections were mounted in aqueous media and analysed by standard light microscopy. Neurons were counted by an investigator blinded to the initial intervention. The mean neuronal densities were calculated for each rat from counts in at least 10 hippocampal sections in high-power fields of 2500 μm^2, located in the CA1b area of the hippocampus. Images were captured with a Zeiss Axiocam (Carl Zeiss, Jena, Germany) and Axiovision software (Carl Zeiss).

Hippocampal slices

For whole-cell patch-clamp recordings, animals were perfused through the heart with 1–3°C cold sucrose-based artificial cerebrospinal fluid (aCSF) containing (in mM): NaCl, 56; sucrose, 100; KCl, 2.5; NaH_2PO_4, 1.25; $NaHCO_3$, 30; $CaCl_2$, 1; $MgCl_2$, 5; glucose, 20 (95% CO_2/5% O_2) under deep anaesthesia with ketamine (100 mg kg^{-1}) and xylazine (15 mg kg^{-1}). After complete perfusion rats were decapitated, the brain was quickly removed and 300 μM-thick transverse hippocampal slices were prepared with a vibrating blade microtome (Leica VT 1200 S, Solms, Germany) and gradually warmed to 34°C over 30 min in a storage chamber perfused with sucrose–aCSF identical to the one above, but with 26 mM $NaHCO_3$ and 60 mM NaCl (95% CO_2–5% O_2). Slices were then transferred to a holding chamber and equilibrated at room temperature (21°C) for at least 60 min with aCSF containing (in mM): NaCl, 125; KCl, 3.5; NaH_2PO_4, 1.25; $MgCl_2$, 2; $CaCl_2$, 2; $NaHCO_3$, 26; glucose, 15 (pH 7.4; 310 mosmol l^{-1}). In addition, μ-conotoxin MVIIC (3 μM) and μ-agatoxin GIVA (200 nM) were added to irreversibly block high voltage-activated N- and P/Q-type calcium currents (Su *et al.* 2002).

Whole-cell patch-clamp recordings

Hippocampal slices were placed in a submerged recording chamber at 34°C and continuously perfused with oxygenated aCSF containing (in mM): TEA-Cl, 20; sodium methanesulfonate, 115; KCl, 3.5; Hepes, 10; $CaCl_2$, 2; $MgCl_2$, 2; 4-aminopyridine, 4; glucose, 25 (pH 7.4, osmolarity 310 mosmol l^{-1}). In addition, nifedipine (10 μM) was added to block L-type calcium currents. For recording pure I_{CaT}, a possible overlap with R-type calcium current was circumvented by measuring tail currents following the voltage steps at 3 ms after the end of the depolarization pulse (Becker *et al.* 2008). Pyramidal cells in the CA1 field were visualized at 60× magnification using a Nikon FN1 microscope and an infra-red video camera (Hamamatsu, Japan). Recording patch pipettes (2–4 MΩ) were pulled from borosilicate glass on a vertical puller (Narishige, Tokyo, Japan). Intracellular (pipette) solution contained (in mM): caesium methanesulfonate, 105; TEA-Cl, 20; Hepes, 10; BAPTA, 10; $MgCl_2$, 2; $CaCl_2$, 2; sucrose, 25; Na_2-ATP, 4; GTP, 0.3 (pH 7.4). Tight-seal whole-cell recordings were obtained using a patch-clamp amplifier (Axopatch 200A, Molecular Devices, Sunnyvale, CA, USA). The signals were filtered on-line at 5 kHz, digitized at a sampling rate of 10 kHz and stored on hard disk (TL-1 DMA and pCLAMP, Molecular Devices). Series resistance compensation was employed to improve the voltage-clamp control (>70%) so that the maximal residual voltage error did not exceed 5 mV. A liquid junction potential of 5 mV was measured between the intra- and extracellular solutions, and corrected off-line.

Data analysis

I_{CaT} amplitudes were determined from the size of the slow deactivating component of tail currents elicited by 20 ms-long depolarizing step potentials and fitted with a biexponential equation using a Levenberg–Marquard non-linear curve-fitting procedure (Becker *et al.* 2008). I_{CaT} activation curves were constructed from current–voltage (I–V) relationships, normalized, and then fitted by Boltzmann's equation. Steady-state inactivation of I_{CaT} was measured by the use of conventional double-pulse method with V_H of −100 mV and was also fitted by Boltzmann's equation:

$$I/I_{max} = 1/\{1 + \exp[(V_m - V_{0.5})/k]\}$$

where I is the peak current, I_{max} is the peak current when the conditioning pulse was −100 mV, V_m and $V_{0.5}$ are the conditioning potentials and the half-inactivation potentials, respectively, and k is the inactivation slope. The 10–90% rise times of I_{CaT} were measured from current traces evoked by 200 ms-long depolarizing steps. The inactivation time course of I_{CaT} was obtained from these traces by fitting the current decay with a bi-exponential equation of the form:

$$I(t) = A_1(1 - \exp(-t/\tau_f)) + A_2(1 - \exp(-t/\tau_s)),$$

where $I(t)$ is the current amplitude at the time point t after onset of the voltage command, τ_f and τ_s are the fast and slow decay time constants, respectively, and A is the amplitude contribution of the different time constants.

The dose–response curve for nickel block of I_{CaT} was obtained by fitting the data points with a modified Hill function of the form:

$$E = E_{max} c^n / (c^n + IC_{50}^n),$$

where E is the fraction of current blocked, E_{max} is the maximal block, c is the concentration of nickel, n is the Hill coefficient, and IC_{50} is the nickel concentration causing half-maximal block.

All curve fittings were done using a Levenberg–Marquard non-linear curve-fitting procedure.

Statistical analyses

Paired or unpaired Student's t tests were used, as required, for two-sample comparisons. ANOVA was used for comparison of multiple samples. Chi^2 was used for comparison of proportions. Kolmogorov–Smirnov test for normal distribution was used to assess the fitting of values to a normal distribution curve. Values were considered significantly different at $P < 0.05$. All results are plotted as mean ± SEM.

Results

Zinc and ibotenic acid induce loss of hippocampal pyramidal neurons

For histological evaluation, brains were removed and sliced 7–10 days after the I.C.V. injections. Slices were immunolabeled with antibodies against NeuN (see Methods). In saline-injected animals ($n = 11$), both right (ipsilateral to injection) and left hippocampi (contralateral to injection) were intact, without signs of pyramidal cell loss (Fig. 1*Aab*, *D* and *E*). No differences in the average densities of CA1 pyramidal cells between ipsilateral and contralateral hippocampi were found (ipsilateral: 10.7 ± 0.09 neurons (2500 μm)$^{-2}$; contralateral: 10.8 ± 0.15 neurons (2500 μm)$^{-2}$; $P = 0.5$).

It was previously reported that unilaterally I.C.V. injected zinc spreads to all ventricles within an hour and permeates the parenchyma of both hemispheres, accumulating in both hippocampi, though the concentration attained is higher on the ipsilateral side (Takeda *et al.* 1994). In congruency with this finding and with the well-known neurotoxicity of zinc (Choi & Koh, 1998), a severe necrotic lesion extending from the ventricle to the hippocampus was found in the ipsilateral hemisphere of zinc-injected animals ($n = 5$; Fig. 1*Ba*). Maximal damage was observed in the CA1 and CA3 fields. The necrotic lesions induced by zinc did not spread to contralateral hippocampi (Fig. 1*Bb*). However, sporadic pyramidal cell loss and appearance of neurons with shrunken cytoplasm and pyknotic nuclei were evident on that side (Fig. 1*Bb* detail). Compared with CA1 pyramidal cell densities in the saline-injected group, zinc injections caused death of ∼75% of neurons in ipsilateral hippocampi and ∼20% of neurons in the contralateral hippocampi (average densities of cells were 2.5 ± 0.22 and 8.8 ± 0.09 neurons (2500 μm)$^{-2}$, respectively; $P < 0.01$ for both; Fig. 1*D* and *E*).

Expectedly, areas of extensive injury were found within the CA1 and CA3 regions in ipsilateral hippocampi following injection of ibotenic acid ($n = 7$; Fig. 1*Ca*). As in zinc-injected animals, sporadic pyramidal cell loss and damage were evident on the contralateral side (Fig. 1*Cb*). The mean densities of CA1 pyramidal cells in the ipsilateral (2.06 ± 0.34 neurons (2500 μm)$^{-2}$) and contralateral (9.06 ± 0.23 neurons (2500 μm)$^{-2}$) hippocampi were significantly lower than in saline-injected rats ($P < 0.01$ for both) and similar to those in zinc-injected animals ($P = 0.3$ and 0.1, respectively; Fig. 1*D* and *E*).

Zinc causes upregulation of I_{CaT}

We next assessed the magnitude of I_{CaT} in CA1 pyramidal cells in slices removed from saline-injected ($n = 6$), zinc-injected ($n = 31$) and ibotenate-injected rats ($n = 8$), obtained 2–12 days after injections. To that end, we performed whole-cell patch-clamp recordings in conditions of blocked Na^+ and K^+ currents. Likewise, the contribution of high-threshold L-, N- and P/Q-type calcium currents was minimized by adding selective antagonists of the respective calcium channels to the aCSFs (see Methods), and by applying small depolarizing current pulses. The neurons were maintained at a holding potential of −95 mV (to maximize the availability of T-type calcium channels; see below) and subjected to a series of 20 ms-long depolarizing voltage steps from −75 to −35 mV in increments of 5 mV (Fig. 2*A*, left panel). The measured capacitance of neurons in the saline-, zinc- and ibotenic acid-injected animals did not differ significantly (24.8 ± 1.4; 24.2 ± 0.9; 23.9 ± 1.7 pF, respectively), indicating that zinc and ibotenic acid injections did not affect cell size. Thus, for comparative purposes, I_{CaT} are displayed as current size (pA), not as current densities (pA pF^{-1}). Illustrative recordings of I_{CaT} in neurons from the three groups are shown in Fig. 2*A*. To eliminate the putative contribution of the fast deactivating Ni^{2+}-sensitive R-type calcium current to the measured currents (Zamponi *et al.* 1996), amplitudes of I_{CaT} were derived from the slow component of the tail currents following depolarizing steps to −45 mV (Sochivko *et al.* 2002; Su *et al.* 2002; Becker *et al.* 2008; see Methods). I_{CaT} averaged 196.7 ± 25.0 pA in

the saline-injected group ($n = 12$), 323.0 ± 26.7 pA in the zinc-injected group ($n = 57$) and 176.4 ± 14.0 pA in the ibotenate-injected group ($n = 14$). These data, summarized in Fig. 2*C*, show that in neurons from zinc-injected rats, I_{CaT} was 1.6-fold larger than I_{CaT} in neurons from saline-injected rats ($P < 0.01$), and 1.8-fold larger than I_{CaT} in neurons from ibotenate-injected rats ($P < 0.01$). No significant difference in amplitudes of I_{CaT} was found between neurons from saline-injected rats and those from ibotenate-injected rats ($P = 0.24$; Fig. 2*C*).

The curves depicting I_{CaT} activation and steady-state inactivation *versus* voltage were similar in all three groups of animals (Fig. 2*B*). The $V_{0.5}$ values of activation for the saline-, zinc- and ibotenate-injected rats were -33.4 ± 0.8, -34.4 ± 0.7 and -34.2 ± 0.8 mV, respectively ($P = 0.5$; Fig. 2*D*). The $V_{0.5}$ values of steady-state inactivation were 68.3 ± 1.1, -66.5 ± 1.2 and -65.3 ± 1.0 mV, respectively ($P = 0.4$; Fig. 2*E*). We further compared the activating and deactivating kinetics of I_{CaT} in neurons from saline-injected *versus* zinc-injected rats. To that end, we elicited I_{CaT} values by 200 ms-long depolarizing voltage

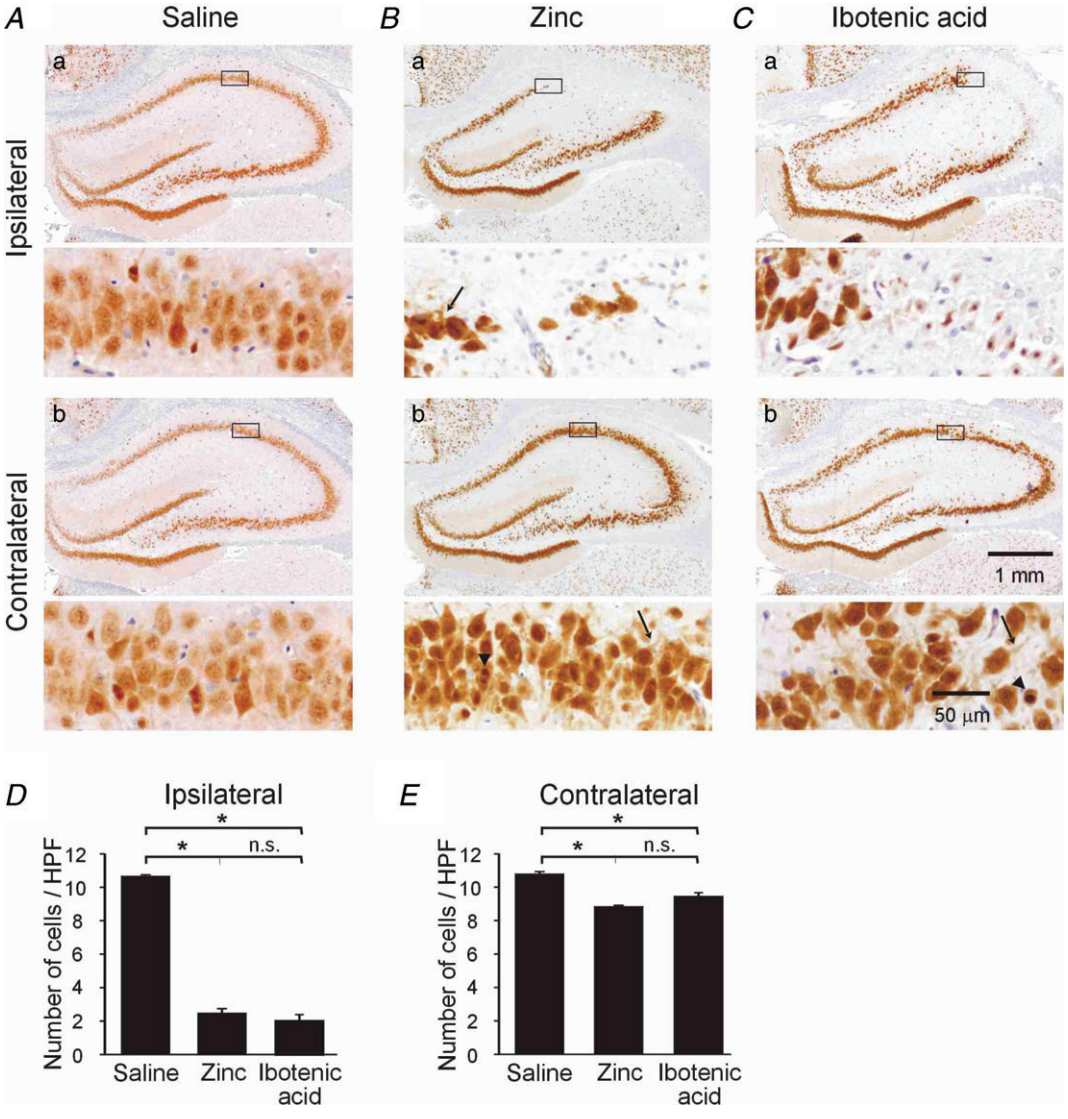

Figure 1. I.C.V. zinc injection induces hippocampal neuronal cell loss, similarly to injection of ibotenic acid
A–C, hippocampal slices immunolabeled for NeuN from rats injected I.C.V. with saline (*A*), zinc (*B*) and ibotenic acid (*C*). Each panel shows at low (top) and at high magnification (bottom) immunolabeled slices from the ipsilateral (*a*) and contralateral hippocampi (*b*) of the same animal. For each slice, the rectangular area shown with high magnification is labeled at the top. Neurons from zinc- and ibotenic acid-injected rats show signs of damage, such as pyknotic nuclei (arrowheads) and shrunken cytoplasms (arrows). *D* and *E*, bar graphs depicting the mean neuronal density in ipsilateral (*D*) and contralateral (*E*) CA1 areas from rats injected with saline, zinc and ibotenic acid. HPF, high power field (2500 mm^2).

steps (Fig. 2*F*) and measured their 10–90% rise time values, as well as the fast (τ_f) and slow (τ_s) decay time constants (see Methods). For voltage pulses to −40 mV (which would minimize activation of residual high voltage-activated calcium currents), the I_{CaT} rise time values in neurons from saline-injected ($n = 5$) and zinc-injected animals ($n = 6$) were similar (7.8 ± 0.1 and 7.3 ± 0.1 ms, respectively; $P = 0.17$; Fig. 2*G*). Likewise,

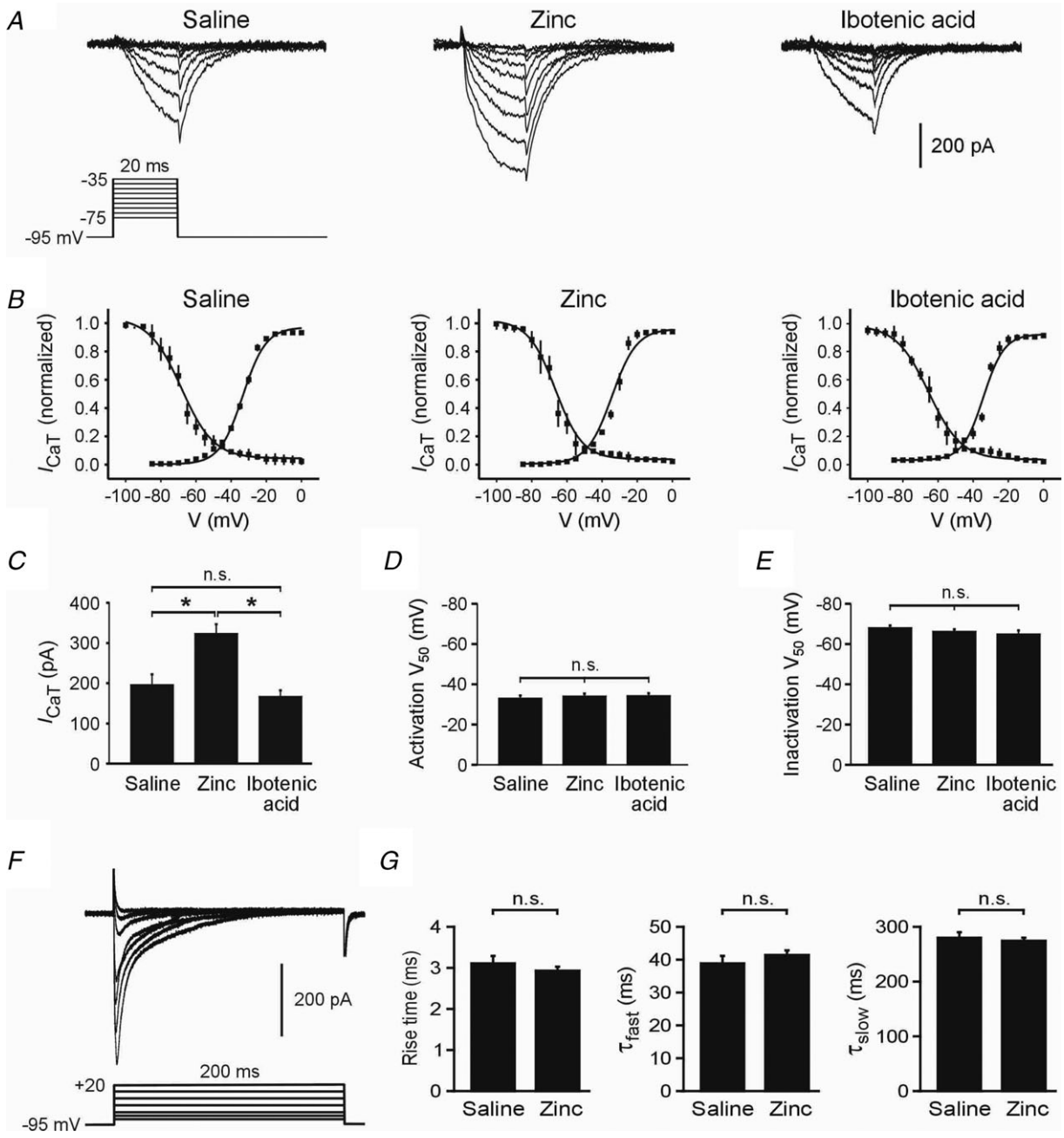

Figure 2. I.C.V. zinc injection upregulates I_{CaT} in CA1 pyramidal cells
A, representative examples of I_{CaT} from saline- (left panel), zinc- (middle panel) and ibotenic acid-injected rats (right panel). Tail currents were measured at −95 mV following 20 ms depolarization steps to different potentials. *B*, normalized I_{CaT} activation and inactivation curves for saline- (left panel), zinc- (middle panel) and ibotenic acid-injected rats (right panel). *C*. Bar graph comparing mean I_{CaT} amplitudes measured at a test pulse potential of −45 mV in saline-, zinc- and ibotenic acid-injected rats. *D*, bar graph showing V_{50} values for I_{CaT} activation in the three groups of neurons. *E*, bar graph showing V_{50} values for I_{CaT} steady-state inactivation in the three groups of neurons. *F*, representative traces of I_{CaT} recorded in response to long command steps from a holding potential of −90 mV to test potentials from −80 to +20 mV in a cell from a zinc-injected rats. *G*, bar graphs comparing rise time values and fast and slow decay time constants between neurons from saline- and zinc-injected rats.

their τ_f (97.3 ± 1.2 and 104.0 ± 1.1 ms, respectively; $P = 0.19$) and τ_s (696.2 ± 5.1 and 678.7 ± 4.8 ms, respectively; $P = 0.28$) were the same (Fig. 2*G*).

Together, these results suggest that zinc-induced upregulation of I_{CaT} in CA1 pyramidal cells is underlain by an increase in the density of T-type calcium channels, rather than by changes in their voltage sensitivity or kinetics.

The amplitude distribution of I_{CaT} values recorded in neurons from saline-injected rats disclosed a normal distribution ($P = 0.9$; mean = 196.7 pA; SD = 86.7 pA; Fig. 3*A*, left panel), with only 8.3% of these neurons expressing I_{CaT} larger than two SDs from the mean (370.1 pA; Fig. 3*B*). The amplitudes of I_{CaT} in neurons from ibotenic acid-injected rats were also normally distributed ($P > 0.05$; Fig. 3*A*, right panel). No neurons expressing I_{CaT} larger than 370.1 pA were encountered in the latter group (Fig. 3*B*). In contrast, the distribution of I_{CaT} amplitudes in neurons from zinc-injected rats was not normal (Fig. 3*A*, middle panel), with a significant fraction of these neurons expressing currents larger than 370.1 pA ($P < 0.001$; Fig. 3*B*). The latter distribution comprised two slightly overlapping normal distributions ($P = 0.9$ and $P = 1$; Fig. 3*A*, middle panel). One distribution had a mean I_{CaT} of 225.0 ± 11.3 pA ($n = 41$; 71.9% of all neurons), which did not differ from the mean I_{CaT} in both control groups ($P = 0.3$; Fig. 3*C*). The second distribution had a mean I_{CaT} of 574.1 ± 25.8 pA ($n = 16$; 28.1% of all neurons), differing significantly from I_{CaT} in both control groups ($P < 0.01$; Fig. 3*C*). The neurons having large I_{CaT}s were similar to the other neurons from zinc-injected rats with respect to cell capacitance (Fig. 3*D*) and series resistance (Fig. 3*E*).

Nickel sensitivity of I_{CaT}

To further characterize I_{CaT} in CA1 pyramidal cells from zinc-injected rats, we studied its sensitivity to blockade by nickel. Nickel has been shown to much more potently block the recombinently expressed $Ca_V3.2$ isoform of T-type calcium channels ($EC_{50} = 13\ \mu M$) than the two other isoforms, $Ca_V3.1$ ($EC_{50} = 216\ \mu M$) and $Ca_V3.3$ ($EC_{50} = 250\ \mu M$; Lee *et al.* 1999). In neurons from zinc-injected animals, Ni^{2+} reduced I_{CaT} in both subgroups (large and small I_{CaT}) by 71.5% (from 544.27 ± 57.7 pA to 157.1 ± 34.2 pA; $n = 4$; $P = 0.0054$) and 75.0% (from 206.5 ± 22.14 pA to 50.4 ± 4.4 pA; $n = 4$; $P = 0.0037$), respectively, similar to the reduction in neurons from saline-injected rats (Fig. 4*A* and *B*). Figure 4*C* depicts the dose–response curves for nickel blockade of I_{CaT} in neurons from saline- and zinc-injected

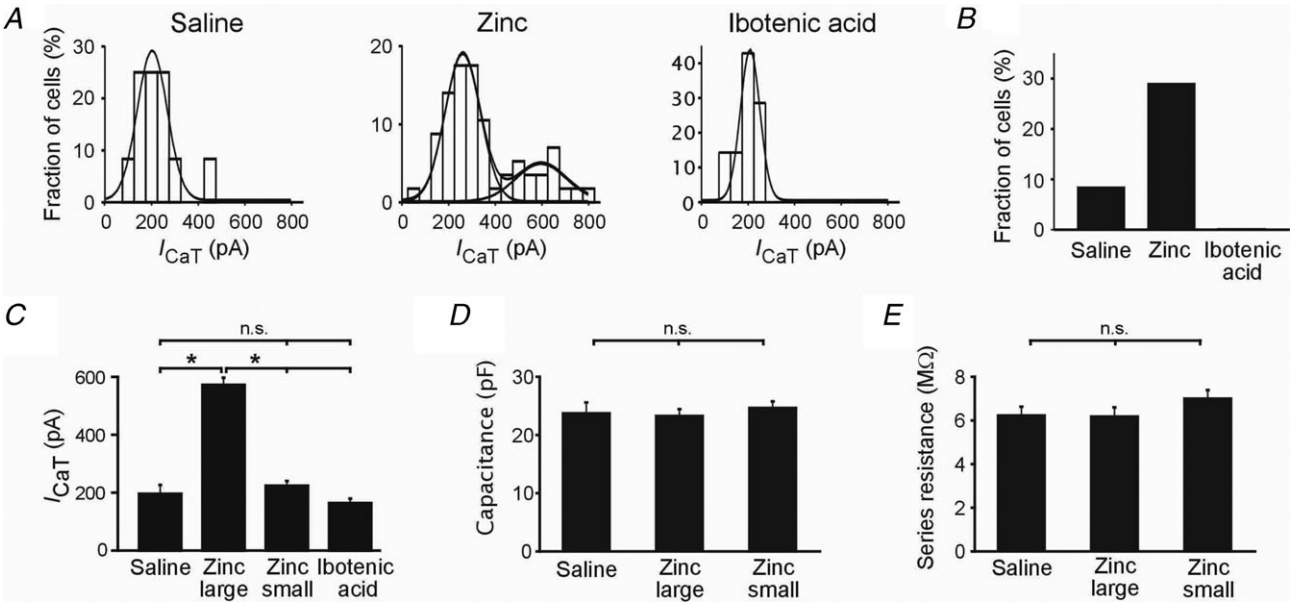

Figure 3. Variation in I_{CaT} amplitudes in zinc-injected CA1 pyramidal cells
A, amplitude distribution histograms of I_{CaT} amplitudes in CA1 pyramidal cells from saline-, zinc- and ibotenic acid-injected animals. The histograms were fitted with Gaussian curves and show the appearance of a subpopulation of cells with larger I_{CaT} in zinc-injected animals. *B*, bar graph showing fraction of neurons in the three groups of animals manifesting I_{CaT} larger than 370.1 pA (mean + 2SDs of I_{CaT} in the saline-injected group). *C*, bar graph comparing I_{CaT} amplitudes (recorded at a test pulse potential of −45 mV) in the two neuron subgroups from zinc-injected animals *versus* I_{CaT} amplitudes in neurons from saline- and ibotenic acid-injected animals. *D*, bar graph showing similar capacitance of the two neuron subgroups from zinc-injected animals and saline-injected animals. *E*, bar graph showing similar series resistance of the two neuron subgroups from zinc-injected animals and saline-injected animals.

rats. The estimated EC_{50} values were $40.45 \pm 8.1\ \mu M$ ($n = 3$) and $35.7 \pm 9.5\ \mu M$ ($n = 5$), respectively, and did not significantly differ from each other ($P = 0.21$; F test comparison). These values are consistent with I_{CaT} being predominantly generated by $Ca_V3.2$ channels in both groups of neurons (Lee *et al.* 1999).

Day-by-day time course of zinc-induced I_{CaT} upregulation

Given that I_{CaT} was markedly upregulated in zinc-injected animals, we sought to determine the precise time course and persistence of this alteration. Figure 5 shows a plot of average I_{CaT} measured in animals killed 1, 2, 3, 4, 6, 9, 12 and 18 days after zinc injection ($n \geq 5$ for each subgroup of neurons; total $n = 71$). The increase in I_{CaT} was evident

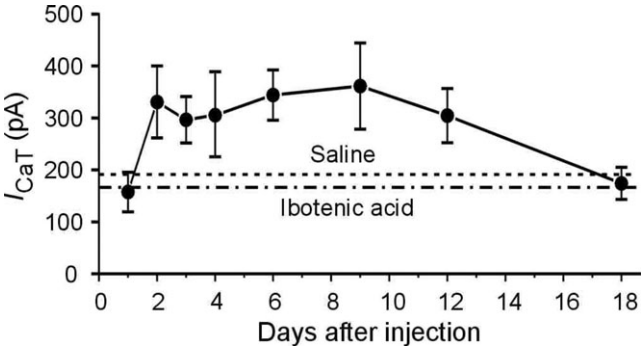

Figure 5. Time course of zinc-induced I_{CaT} increase
Each data point is the mean I_{CaT} amplitude of 5–12 cells from 5–8 animals. The dashed lines represent the mean I_{CaT} amplitudes in neurons from saline- and ibotenic-acid injected rats.

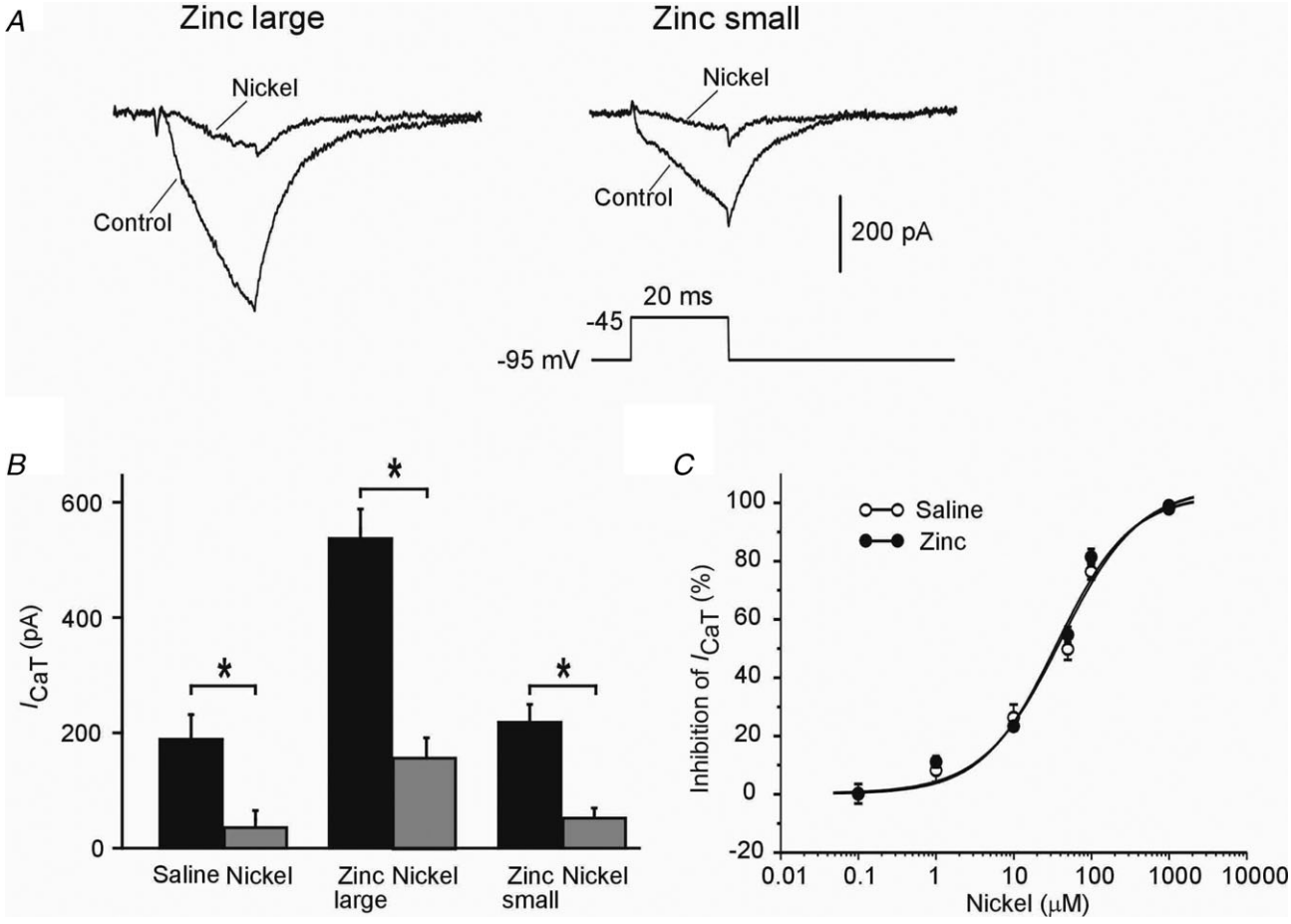

Figure 4. Blockade of I_{CaT} by nickel
A, representative traces of I_{CaT} before (Control) and 5 min after adding 100 μM nickel to the aCSF (Nickel) in the two neuron subgroups from zinc-injected animals. *B*, bar graph showing the similar blocking effect of 100 μM nickel on I_{CaT} in the two neuron subgroups from zinc-injected animals ($n = 4$ for each subgroup) and saline-injected rats ($n = 3$). *C*, concentration–response curve for nickel on I_{CaT} in cells from saline-injected rats ($n = 3$; open circles) and zinc-injected rats ($n = 5$; filled circles). Data were fitted with a Hill equation using a Levenberg–Marquard non-linear curve-fitting procedure. The fitted lines are shown superimposed on the data points for saline- and zinc-injected rats, and are almost indistinguishable.

from day 2 and remained elevated without increasing further for about 2 weeks, after which it returned to baseline.

Acute effect of zinc on I_{CaT}

Finally, we examined the effects of acutely applied zinc on I_{CaT} in CA1 pyramidal cells ($n = 6$) in hippocampal slices obtained from naive rats. Adding 300 μM of zinc to the aCSF rapidly and markedly suppressed I_{CaT} by $94.3 \pm 0.5\%$ (from 238.3 ± 15.7 to 13.6 ± 1.3 pA; $n = 6$; $P < 0.05$; Fig. 6*A*–*C*). This effect was readily reversible upon zinc washout (data not shown; Traboulsie *et al.* 2007). These data show that zinc exerts a dual action on I_{CaT}, blocking it acutely, but also triggering processes leading to its eventual upregulation.

Discussion

In this study we show that exposing rat hippocampi *in vivo* to zinc or ibotenic acid causes comparable pyramidal cell loss. Despite the similarity in neuronal damage, zinc, but not ibotenic acid, induces a long-term upregulation of I_{CaT} in a substantial subset of surviving CA1 pyramidal cells. These findings suggest that the increase in I_{CaT} in zinc-injected animals is due to a unique action of zinc itself, rather than reflecting a non-specific alteration associated with neurotoxicity.

Intriguingly, we found that only a subset of neurons from zinc-injected rats, comprising ~28% of the sampled population, displayed an augmented I_{CaT}. The reasons for this differential modulation remain unclear. Although there was no apparent clustering of neurons manifesting a large I_{CaT} in particular slices, it is possible that following I.C.V. injection some neurons are exposed to larger concentrations of zinc than others or are more vulnerable to its action, as is also indicated by the sporadic death of neurons on the contralateral side of injection.

The upregulation of I_{CaT} became evident only during the second day after zinc I.C.V. injection, after which I_{CaT} remained elevated for another 2 weeks without increasing further and then declined to baseline level (Fig. 5). The latency period likely is due to the time required for zinc to exert its modulatory action. This action may be exerted intracellularly, as zinc readily enters neurons through multiple receptor-operated and voltage-gated channels and via carrier-mediated transport (Colvin *et al.* 2003).

The potent suppression of I_{CaT} by 100 μM nickel (Fig. 4*A* and *B*) in neurons expressing either large or small I_{CaT} indicates that $Ca_V3.2$ is the predominant T-type calcium channel subunit in CA1 pyramidal cells from zinc-treated rats, as is likely the case in normal CA1 pyramidal cells. Though further experiments are necessary to characterize the mechanism underlying the modulation of I_{CaT} by zinc, we speculate that it involves transcriptional upregulation of $Ca_V3.2$. Indeed, we have recently found that cytosolic zinc enhances transcription of $Ca_V3.2$ in NG108–15 cells via its binding to MTF-1 (A. J. Becker, K. M. J. van Loo, Y. Yaari and S. Schoch, unpublished observations). Whatever the mechanism, the long-term upregulation of I_{CaT} in CA1 pyramidal cells exposed to zinc contrasts markedly with the fact that zinc applied acutely is a potent blocker of I_{CaT} in these neurons (Fig. 6), similar to its reported effect in other preparations (Nelson *et al.* 2007; Traboulsie *et al.* 2007; Kang *et al.* 2010).

We have previously shown in both rats and mice that a single episode of SE induced by the convulsant pilocarpine leads to a marked upregulation of I_{CaT} induced by $Ca_V3.2$ promoter activation (Su *et al.* 2002; Becker *et al.* 2008). The mechanism coupling SE to $Ca_V3.2$ transcription has not been clarified, but our study suggests that involvement of zinc is a likely option. In line with this hypothesis, it was shown that pilocarpine-induced SE

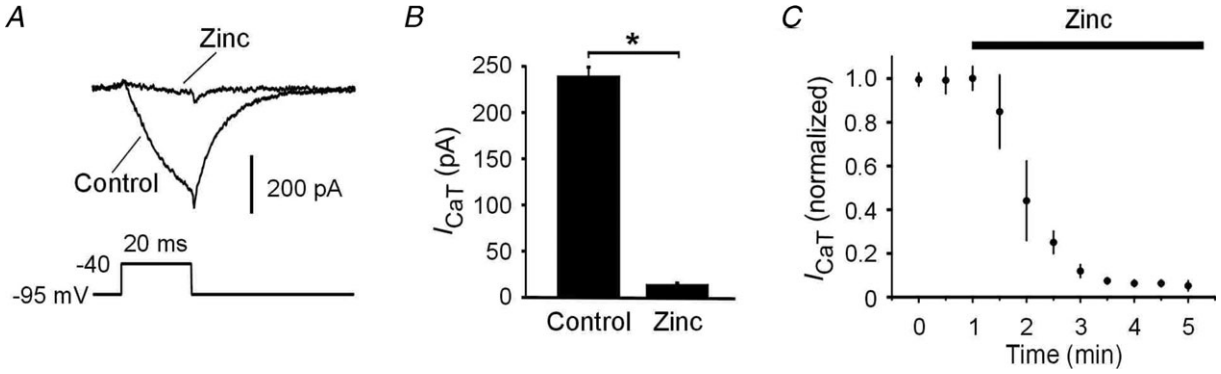

Figure 6. Acute effects of zinc on I_{CaT} in ordinary CA1 pyramidal cells
A, representative traces of I_{CaT} before (Control) and 5 min after adding 300 μM zinc to the aCSF (Zinc). *B*, bar graph showing the marked suppression of I_{CaT} (recorded at a test pulse potential of −45 mV) by 300 μM zinc ($n = 6$). *C*, graph showing the rapid time course of I_{CaT} block by 300 μM zinc (application marked by bar). I_{CaT} amplitudes were normalized to initial amplitude ($n = 6$).

causes accumulation of free zinc in CA1 pyramidal cell somata within 24 h (Suh *et al.* 2001). The somatic zinc may originate from the enhanced release of vesicular zinc during seizure discharges (Suh *et al.* 2001). Alternatively, or in addition, zinc may be released locally in the soma from metallothioneins by nitric oxide or other free radicals (Cuajungco & Lees, 1998) that are produced in excess during SE (Milatovic *et al.* 2002). Given that I_{CaT} upregulation is likely a critical step in epileptogenesis following pilocarpine-induced SE (Becker *et al.* 2008), it would be of utmost importance to clarify further the molecular mechanisms by which zinc upregulates I_{CaT}.

References

Becker AJ, Pitsch J, Sochivko D, Opitz T, Staniek M, Chen CC, Campbell KP, Schoch S, Yaari Y & Beck H (2008). Transcriptional upregulation of Cav3.2 mediates epileptogenesis in the pilocarpine model of epilepsy. *J Neurosci* **28**, 13,341–13,353.

Besser L, Chorin E, Sekler I, Silverman WF, Atkin S, Russell JT & Hershfinkel M (2009). Synaptically released zinc triggers metabotropic signaling via a zinc-sensing receptor in the hippocampus. *J Neurosci* **29**, 2890–2901.

Choi DW & Koh JY (1998). Zinc and brain injury. *Annu Rev Neurosci* **21**, 347–375.

Colvin RA, Fontaine CP, Laskowski M & Thomas D (2003). Zn^{2+} transporters and Zn^{2+} homeostasis in neurons. *Eur J Pharmacol* **479**, 171–185.

Cousins RJ, Liuzzi JP & Lichten LA (2006). Mammalian zinc transport, trafficking, and signals. *J Biol Chem* **281**, 24,085–24,089.

Cuajungco MP & Lees GJ (1998). Nitric oxide generators produce accumulation of chelatable zinc in hippocampal neuronal perikarya. *Brain Res* **799**, 118–129.

Evstratova A & Toth K (2011). Synaptically evoked Ca^{2+} release from intracellular stores is not influenced by vesicular zinc in CA3 hippocampal pyramidal neurons. *J Physiol* **589**, 5677–5689.

Frederickson CJ, Koh JY & Bush AI (2005). The neurobiology of zinc in health and disease. *Nat Rev Neurosci* **6**, 449–462.

Kang HW, Vitko I, Lee SS, Perez-Reyes E & Lee JH (2010). Structural determinants of the high affinity extracellular zinc binding site on $Ca_V3.2$ T-type calcium channels. *J Biol Chem* **285**, 3271–3281.

Kay AR & Toth K (2006). Influence of location of a fluorescent zinc probe in brain slices on its response to synaptic activation. *J Neurophysiol* **95**, 1949–1956.

Lee JH, Gomora JC, Cribbs LL & Perez-Reyes E (1999). Nickel block of three cloned T-type calcium channels: low concentrations selectively block α_{1H}. *Biophys J* **77**, 3034–3042.

Lee JY, Kim YJ, Kim TY, Koh JY & Kim YH (2008). Essential role for zinc-triggered p75NTR activation in preconditioning neuroprotection. *J Neurosci* **28**, 10,919–10,927.

Lutsky I, Aizer F & Mor N (1984). The Sabra rat: definition of a laboratory animal. *Isr J Med Sci* **20**, 603–612.

Milatovic D, Gupta RC & Dettbarn WD (2002). Involvement of nitric oxide in kainic acid-induced excitotoxicity in rat brain. *Brain Res* **957**, 330–337.

Molnar P & Nadler JV (2001). Synaptically-released zinc inhibits N-methyl-D-aspartate receptor activation at recurrent mossy fiber synapses. *Brain Res* **910**, 205–207.

Nakashima AS & Dyck RH (2009). Zinc and cortical plasticity. *Brain Res Rev* **59**, 347–373.

Nelson MT, Woo J, Kang HW, Vitko I, Barrett PQ, Perez-Reyes E, Lee JH, Shin HS & Todorovic SM (2007). Reducing agents sensitize C-type nociceptors by relieving high-affinity zinc inhibition of T-type calcium channels. *J Neurosci* **27**, 8250–8260.

Park JA, Lee JY, Sato TA & Koh JY (2000). Co-induction of p75NTR and p75NTR-associated death executor in neurons after zinc exposure in cortical culture or transient ischemia in the rat. *J Neurosci* **20**, 9096–9103.

Perez-Reyes E (2003). Molecular physiology of low-voltage-activated t-type calcium channels. *Physiol Rev* **83**, 117–161.

Qian J, Xu K, Yoo J, Chen TT, Andrews G & Noebels JL (2011). Knockout of Zn transporters Zip-1 and Zip-3 attenuates seizure-induced CA1 neurodegeneration. *J Neurosci* **31**, 97–104.

Sensi SL, Paoletti P, Bush AI & Sekler I (2009). Zinc in the physiology and pathology of the CNS. *Nat Rev Neurosci* **10**, 780–791.

Sochivko D, Pereverzev A, Smyth N, Gissel C, Schneider T & Beck H (2002). The $Ca_V2.3$ Ca^{2+} channel subunit contributes to R-type Ca^{2+} currents in murine hippocampal and neocortical neurones. *J Physiol* **542**, 699–710.

Su H, Sochivko D, Becker A, Chen J, Jiang Y, Yaari Y & Beck H (2002). Upregulation of a T-type Ca^{2+} channel causes a long-lasting modification of neuronal firing mode after status epilepticus. *J Neurosci* **22**, 3645–3655.

Suh SW, Thompson RB & Frederickson CJ (2001). Loss of vesicular zinc and appearance of perikaryal zinc after seizures induced by pilocarpine. *Neuroreport* **12**, 1523–1525.

Takeda A, Sawashita J & Okada S (1994). Localization in rat brain of the trace metals, zinc and manganese, after intracerebroventricular injection. *Brain Res* **658**, 252–254.

Traboulsie A, Chemin J, Chevalier M, Quignard JF, Nargeot J & Lory P (2007). Subunit-specific modulation of T-type calcium channels by zinc. *J Physiol* **578**, 159–171.

Vogt K, Mellor J, Tong G & Nicoll R (2000). The actions of synaptically released zinc at hippocampal mossy fiber synapses. *Neuron* **26**, 187–196.

Zamponi GW, Bourinet E & Snutch TP (1996). Nickel block of a family of neuronal calcium channels: subtype- and subunit-dependent action at multiple sites. *J Membr Biol* **151**, 77–90.

Author contributions

The experiments were performed in the laboratories of Y.Y. in the Faculty of Medicine of the Hebrew University, Jerusalem, Israel; and of A.J.B. in the Department of Neuropathology, University of Bonn Medical Center, Bonn, Germany. D.E. and F.B. contributed to the conception and design of experiments, collection, analysis and interpretation of data, and drafting and

revision of the paper. M.D., J.P. and K.V. contributed to the collection, analysis and interpretation of data. A.J.B. contributed to the conception and design of experiments, analysis and interpretation of data, and drafting of the paper. Y.Y. contributed to the conception and design of experiments, interpretation of data, and drafting and revision of the article. All authors approved the final version of the manuscript.

Acknowledgements

This study was supported by SFB TR3, the German-Israeli Foundation for Scientific Research and Development (GIF), the Humboldt Foundation (F.B.), and the Henri J. and Erna D. Leir Chair for Research in Neurodegenerative Diseases (Y.Y.).